Progress In Electromagnetics Research, Vol. 178, 1–12, 2023

Reservoir Computing and Task Performing through Using High-β Lasers with Delayed Optical Feedback

Tao Wang[1, *], Can Jiang[2], Qing Fang[2], Xingxing Guo[1], Yahui Zhang[1], Chaoyuan Jin[3, 4], and Shuiying Xiang[1, *]

Abstract—Nonlinear photonic sources including semiconductor lasers have been recently utilized as ideal computation elements for information processing. They supply energy-efficient way and rich dynamics for classification and recognition tasks. In this work, we propose and numerically study the dynamics of complex photonic systems including high-β laser element with delayed feedback and functional current modulation, and employ nonlinear laser dynamics of near-threshold region for the application in time-delayed reservoir computing. The results indicate a perfect (100%) recognition accuracy for the pattern recognition task and an accuracy about 98% for the Mackey-Glass chaotic sequences prediction. Therefore, the system shows an improvement of performance with low-power consumption. In particular, the error rate is an order of magnitude smaller than previous works. Furthermore, by changing the DC pump, we are able to modify the number of spontaneous emission photons of the system, which then allows us to explore how the laser noise impacts the performance of the reservoir computing system. Through manipulating these variables, we show a deeper understanding on the proposed system, which is helpful for the practical applications of reservoir computing.

1. INTRODUCTION

With the developments of the Internet of Things (IoT) and big data, there is a growing demand for innovative approaches in information processing. Reservoir computing (RC), due to the ability of simplifying the implementation of recurrent neural networks [1–3], has been studied intensively in the past several decades [4–7]. The conventional RC architecture is a real network and typically featured by a large number of nonlinear nodes, and we call this kind of RC as spatially distributed RC (SDRC) [6]. SDRC has been successfully demonstrated through using the arrays of semiconductor optical amplifiers (SOA) [8], coupled photonic emitters (CPE) [9], and silicon photonic chip (SPC) [10]. However, these fully implemented reservoir architectures with a high number of nodes bring various technical challenges.

Alternatively, the innovative concept of a virtual network for RC using a single nonlinear node with a time delay feedback loop has been proposed recently [11], and it is classified as a time-delay RC (TDRC) [12–15]. In comparison with SDRC, TDRC can further simplify the energy-efficient design and allows people to use a single photonic node in combination with a large number of virtual nodes spreading over different locations in a time-delay line [16]. Finally, the number of nodes in the architecture can be modified by changing the length of delay lines. This method can effectively alleviate the physical node/connectivity restrictions of SDRC. Up to now, TDRC has been implemented in different schemes including electronics [11, 17], optoelectronics [18–20], and optics [21–23]. These implementations have shown enhanced performance in benchmark tasks such as Mackey-Glass and Santa-Fe temporal series,

Received 4 April 2023, Accepted 10 July 2023, Scheduled 23 July 2023

* Corresponding authors: Tao Wang (twang6@xidian.edu), Shuiying Xiang (syxiang@xidian.edu.cn).

[1] State Key Laboratory of Integrated Service Networks, Xidian University, Xian 710071, China. [2] School of Electronics and Information, Hangzhou Dianzi University, Hangzhou 310018, China. [3] College of Information Science and Electronic Engineering, Zhejiang University, Hangzhou 310007, China. [4] International Joint Innovation Center, Zhejiang University, Haining 314400, China.

whereas in real-world tasks, e.g., optical channel equalization due to dispersion induced power fading, TDRCs have offered a power-efficient alternative to digital signal processing [24].

The computation mechanism of TDRC originates from the nonlinear transform of the information to be processed onto a high-dimensional state space, assisted by the fading memory properties [25]. Through increasing the operating bandwidth of photonic systems and operating the hardware-efficient photonic topologies, people can target at high information processing speed. In this sense, photonic RCs are ideal candidates for analog processing of optical communication signals. Among different optical TDRC schemes, the system of semiconductor laser (SL) with time-delayed feedback has been used for generating broadband chaotic signals for applications such as chaotic encryption and physical random number generation, by biasing the SL well above the lasing threshold [26–28]. Semiconductor lasers are compact and efficient light sources that offer several unique advantages including small size, fast response, low power consumption, and high efficiency [29, 30]. SL-based TDRC systems can exhibit enhanced dynamical bandwidth emission in the presence of an additional optical injection signal [31, 32].

In this work, we numerically investigate a photonic reservoir computing scheme based on a high-β (refers to $\beta \geq 10^{-2}$ [33]) semiconductor laser which is operated near threshold region. High-β lasers possess small footprint and high efficiency for information processing [33], favoring the development of RC-based neuromorphic visual systems towards high speed, low consumption, and easy integration [34]. The main idea of this work is based on the delayed optical feedback and external carrier modulation, and considers the lasing transition region where the amplified spontaneous emission photons enable spiking dynamics in temporal [35, 36]. We prove that the novel TDRC is not only efficient in dealing with several bench-marking tasks, including pattern recognition and Mackey-Glass chaotic sequences prediction, but the power consuming is also much lower than the previous ones by using low-β lasers. In addition, we pay more attention to the impact of spontaneous emission noise on the performance of the TDRC system. The study could be proved valuable in the development and optimization of TDRC system in the future.

2. COMPUTATIONAL CONCEPT AND MODEL

The scheme of the proposed TDRC based on a high-β semiconductor laser (SL) is shown in Fig. 1, where the RC is made up by three parts: input layer, hidden layer, and output layer. In the input layer, each of the discrete inputs $u(k)$ is maintained for an input time T to produce a continuous signal $\widetilde{u}(t) = u(n)$ for $t \in [(k-1)T, T]$, where T is the operation time of each sampling time, and it is chosen close to the delay time τ in the feedback loop. Then input signal $\widetilde{u}(t)$ is subsequently multiplied by a step function $M(t)$ called input mask as well as a scaling factor (γ, it is a fixed random sequences), and the fluctuation range is -1, 1. This process is often called as masking, which enables the variable signal at different virtual nodes, so that the information can be read out [18]. The resulting signal $I_M(t)$ is transformed into the input signal and then coupled into the hidden layer through the modulator.

The hidden layer also refers to the reservoir part, through dividing the delay loop (τ) into N virtual

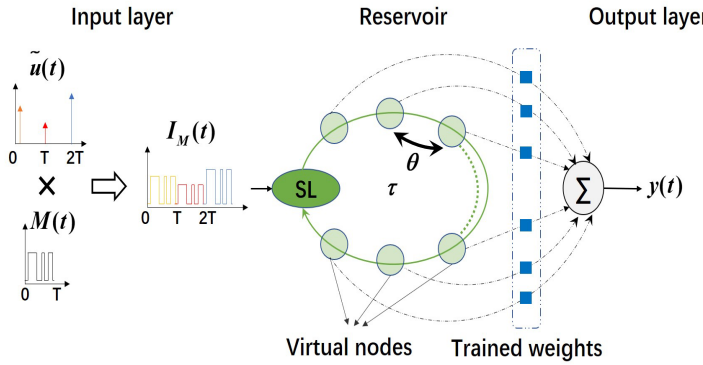

Figure 1. A photonic RC created with a high-β SL subjects to time-delayed optical feedback, with N virtual nodes defined by their equidistant time separation θ.

nodes with spacing θ and $\tau = N\theta$. θ is the node separation which determines the time of the nonlinear node that responds to the time-multiplexed input. In detail, if θ is larger than the intrinsic response time of the reservoir nodes, the latter response has enough time to settle down at a certain state [37]. However, if θ is chosen small in comparison with the response time, the response of each nonlinear node will be always on a transient, with each having a motion coupled to its close neighbors [11]. In addition, the amplitudes of the mask between neighboring θ are often selected randomly from a uniform distribution [37]. Then, the time-multiplexed input signal with the imprinted mask drives the different virtual nonlinear nodes.

For the output layer, the output is interpreted as the state of the virtual network node, and the internal connection matrix, like the input matrix, is also a random sequence that is fixed and fluctuates at $(-1, 1)$. The output layer is a weighted and linear summation stage of the transient responses of different virtual nodes. Different from the input matrix and internal connection matrix, the output matrix has to be trained. The linear least square method is used to minimize the mean square error between the target and predicted values, which can be usually determined by using computer offline training or programmable gate array on-line training. The optical signal is finally post processed in an offline procedure.

In order to properly simulate the proposed TDRC system based on a semiconductor microcavity laser with $\beta = 10^{-2}$, we adopt a newly developed *Stochastic Simulator* (S-S) [38] by inserting the function modulation and feedback terms. S-S is specified as a semiclassical model, which can efficiently describe the dynamics for the lasers from macro- to microscale [36]. This model is unique in that it allows for the separate characterization of stimulated and spontaneous emission, which is different from the non-stochastic approaches. By separating different channel emissions, the S-S model allows for more accurate analysis of laser dynamics. In addition, although the conventional rate equations possess the indubitable merit of providing a wealth of information about laser dynamics, they fail to simulate the dynamics around threshold region, in particular for high-β lasers, since people just introduce the averaged background noisy field into the lasing mode [39]. This incorrect description may also lead people to overlooking the threshold region without any further consideration. In this work, we focus on the temporal dynamics of lasing transition region, which is often ignored when laser is used for practical applications, due to the poor quality of coherence. However, for high-β lasers, this region is very broad and shows spike dynamics, possessing the potential in the application of reservoir computing.

In terms of model, the detail recurrence relations between different physical processes have been well defined in [38] with the optical feedback added as in [36]. In addition to the parameters detailed in previous work [36, 38], we set the spontaneous emission coupling factor β of semiconductor laser to 10^{-2} and ideally make the delay length to 0.6 m, which is corresponding to $\tau = 4$ ns time delay. For the Mackey-Glass chaotic sequences prediction, the input signal is composed of $2.5P_{th} + 5 \times$ Mackey-Glass chaotic sequences (P_{th} is the so-called threshold pump [40]).

To evaluate the performance of the proposed TDRC system, the tests of *pattern recognition* and *Mackey-Glass chaotic sequence prediction* have been carried out. The input dataset is composed of 7000 samples, of which 5000 samples are used for training and 2000 samples for testing. The prediction performance of the system can be usually quantified by computing the normalized mean squared error (NMSE) between the target data y_d and RC system output y_{out}, which is defined by [16]:

$$\mathrm{NMSE} = \frac{1}{L}\frac{\sum_{n=1}^{L}(y_d(n) - y_{out}(n))^2}{\sigma(y_d)} \tag{1}$$

where n is the subscript value of the data index, L the total data set, y_{out} the output value of the RC system, y_d the original data, and $\sigma(\cdot)$ the variance of the original signal.

3. PERFORMANCE CHARACTERIZATION OF TDRC SYSTEM USING HIGH-β LASERS

In this section, we will investigate the two different tasks of pattern recognition and Mackey-Glass chaotic sequences prediction, respectively, and analyze the influences of scaling factor, number of virtual nodes,

injection pump strength, and feedback strength on the prediction performance, and then the memory capacity of the RC is also investigated. During the simulation, regression regularization parameters are used to optimize the performance of each task.

3.1. Pattern Recognition Task

The RC system is first used for a pattern recognition task, as shown in Fig. 2. The target of this task is regenerate the original input signal from the output layer. We set the scaling factor to 0.51, and make the virtual nodes $N = 64$. For the feedback, the strength is defined by $\eta = S_{inj}/S_{out}$ (S_{inj} indicates the photon number fed back into the laser, and S_{out} is the photon number outcoupled from the cavity) and is set to 0.2. It is worth to mention that the laser is biased at the position of $P_{DC} = 2.5P_{th}$, which is still in the lasing transition region. As mentioned before, the S-S model is more effective in describing the laser dynamics within this transition region, since it gives more attention to the dynamics of spontaneous emission noise. As shown by Fig. 2(a), the temporal signal pattern indicated by the red curve is the original signal, and the blue curve is the predicted result by the TDRC system. After comparing them statistically, we can observe that the predicted signal matches the original pattern well, and the minimum NMSE value goes down to 0.0467. Fig. 2(b) shows the difference between the original and predicted signals. The smaller NMSE indicates that the TDRC reaches a better prediction effect on the pattern recognition task than the previous work [41].

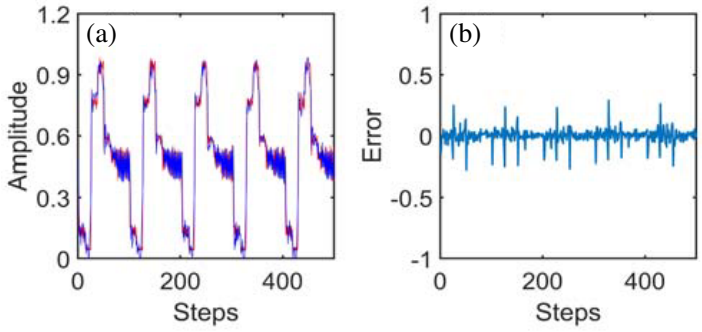

Figure 2. (a) Temporal waveforms of the original signal (red curve) and the predicted signal (blue curve) through TDRC system obtained under $\gamma = 0.81$, $N = 64$, $\eta = 0.2$ and $P_{DC} = 2.5P_{th}$; (b) Temporal errors after predicting by using TDRC.

In order to further explore the influences of different parameters on the predicted performance of the TDRC system, we carry out a series of investigations by changing the scaling factor, number of virtual nodes, injection strength, and feedback strength, respectively. Fig. 3(a) shows the variation of NMSE as the function of scaling factor γ, under the condition of $N = 64$, $\eta = 0.2$ and $P_{DC} = 2.5P_{th}$. The function curve shows the value of NMSE first decreases with γ, reaching the minimum value at $\gamma = 0.81$, then goes up again. Thus, we can easily find that the optimized prediction result is achieved when $\gamma = 0.81$, where the NMSE reaches the minimum value, 0.046. Then, the change of NMSE with the number of virtual nodes is plotted by setting $\gamma = 0.81$. As shown in Fig. 3(b), the NMSE values keep decreasing with the number of virtual nodes, but in different levels. Another slope is observed when $N > 64$, which indicates that the decaying becomes very slow. After that, the effect of DC pump is also investigated by fixing $N = 64$. It is obvious that NMSE gives a substantial reduction when $P_{DC} < 1.7P_{tn}$ (Fig. 3(c)), which is mainly attributed by the reduction of spontaneous emission noise. But it keeps almost constant when $P_{DC} > 1.7P_{tn}$. Fig. 3(d) is the influence of feedback strength on NMSE, and the function curve exhibits a similar line shape to the result of Fig. 3(c). The value of NMSE cannot be further reduced when $\eta > 0.15$.

To further dynamically identify the optimized parameters, the simultaneous dependence of NMSE on the feedback strength and the virtual node number is investigated by plotting the distribution of NMSE. As shown in Fig. 4(a), we find that NMSE achieves very small values with the order of 10^{-2} in

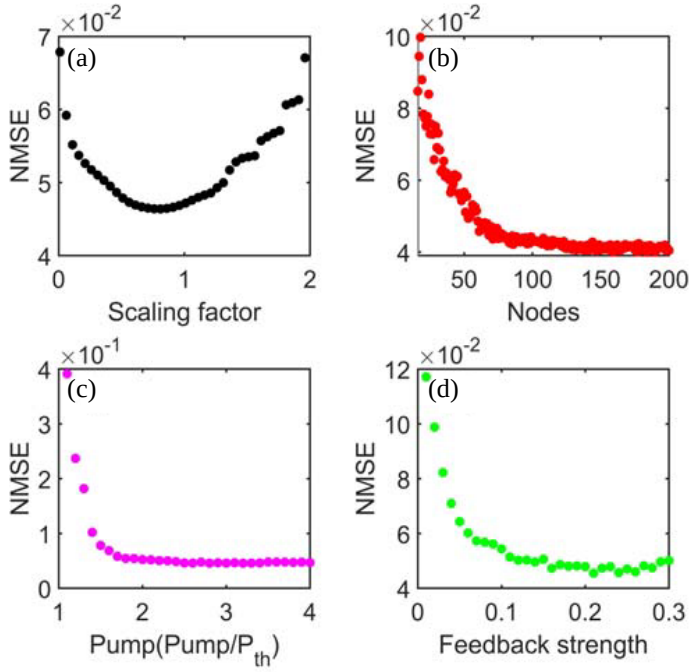

Figure 3. Influences of different parameters on the pattern recognition prediction: (a) scaling coefficient, (b) number of virtual node, (c) DC pump strength and (d) feedback strength.

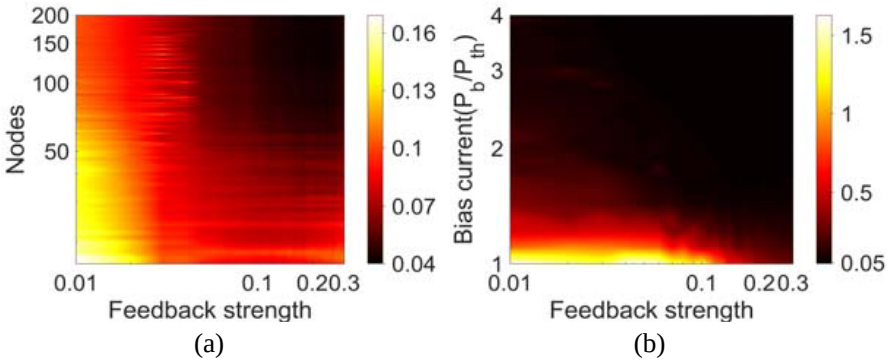

Figure 4. NMSE for the pattern recognition task (a) as a function of feedback strength and virtual node number, as well as (b) a function of feedback strength and DC pump using the high-β-laser-based TDRC system.

the region of $\eta > 0.05$ and $N > 50$. For the conventional TDRCs using macroscopic lasers, it has been recognized that too small feedback level cannot supply sufficient memory for this task, and too large feedback can introduce system oscillation thereby degrades the consistency property [42–44]. However, our results reveal that high-β lasers enable TDRC to still keep good consistency even η goes up to 0.30, showing a distinguished advantage. As for the virtual node, if the number is too small, there only a few sampled data which increases the fluctuations of the NMSE. However, too many virtue nodes will have no obvious effect on NMSE and even bring subtly adverse impact [20].

Fig. 4(b) is the simultaneous dependence of TDRC performance on the DC pump and feedback strength. Interestingly, the results clearly show that NMSE can directly keep small values without the consideration of feedback strength if $P_{DC} > 1.3P_{th}$. In the opposite direction, the NMSE shows larger number due to the large components of spontaneous noise, which degrades the performance of the system. To sum up, the feedback strength, the number of virtual nodes, and the DC pump all impact

the value of NMSE. However, if the reservoir works in the region with $P_{DC} > 1.3P_{th}$ and $N > 50$, the better prediction performance of the pattern recognition task can be obtained over a larger range of feedback strength. This remarkable feature enables the reservoir to be more flexible for the pattern recognition task.

3.2. Mackey-Glass Chaotic Sequence Prediction Task

Next, the TDRC system is also explored to predict the Mackey-Glass chaotic sequences, and the aim of this task is to perform single-point-prediction of chaotic data. In this simulation, the discretization time step is 0.3 ns. Additionally, the fixed scaling factor $\gamma = 0.81$, virtual nodes $N = 64$, feedback strength $\eta = 0.2$, and the DC pump is still $2.5P_{th}$. Then 7000 data points are generated by the high-β laser, and 5000 points of the data for training and the left 2000 points for testing.

Figure 5(a) shows the typical temporal waveforms for this task, and the predicted waveform (red curve) is obtained under the condition with $P_{DC} = 2.5P_{th}$, $\eta = 0.2$, and $N = 64$. We note that the red line almost coincides with the blue line, and there is only slight difference at the sharp positions. Therefore, the temporal deviations between the original and predicted signals are very small, and the errors are much smaller than the case of pattern recognition task, as shown in Fig. 5(b).

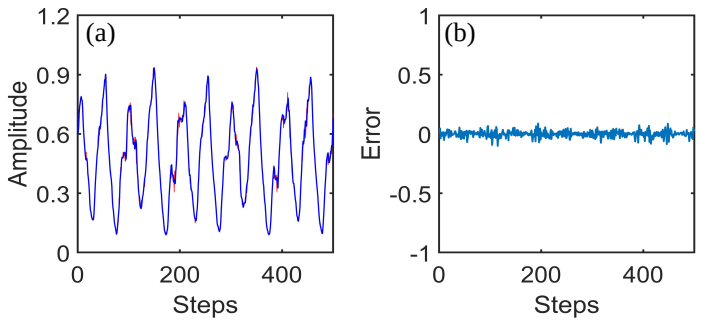

Figure 5. (a) Mackey-Glass sequence prediction time domain; (b) output matrix weights.

Same as the task of pattern recognition, we also investigate the effects of scaling factor, number of virtual nodes, injection pump strength, and feedback strength on the prediction performance of Mackey-Glass chaotic sequences. Fig. 6(a) is the effect of the scaling factor on NMSE, and the minimum NMSE of 0.015 is obtained when the scanning coefficient is 0.41. Fig. 6(b) shows that a fast decaying of NMSE is observed within the region with $N < 80$, then a very slow decaying with small fluctuations is presented when $N > 80$, indicating a saturation of the performance improvement when $N > 80$. Fig. 6(b), Fig. 6(c), and Fig. 6(d) display the effects of DC pump and feedback strength on NMSE, respectively. In general, higher NMSE values ($\sim 10^{-2}$) are obtained at the beginning, then gradually decrease with DC pump and feedback strength, but the function curves display similar line shapes. When $P_{DC} > 2.5P_{th}$ and $\eta > 0.2$, NMSE achieves the minimum value. When those parameters go up to even higher values, NMSE values keep almost constant.

Fig. 7(a) shows the mapping diagram of NMSE distribution with the virtual node number and feedback strength, under the condition of $P_{DC} = 2.5P_{th}$. We note that the TDRC system has better performance than that of pattern recognition task, due to much smaller NMSE values. Closer observation indicates that the minimum NMSE is located in the region with $N > 60$ and $\eta > 0.2$. When the feedback strength is significantly lower, NMSE consistently remains at a higher value, irrespective of the number of virtual nodes in the system.

Fig. 7(b) is the mapping of NMSE distribution depending on the DC pump and feedback strength, under the condition of $N = 64$. When the laser is operated at $P_{DC} = P_{th}$, due to the large component of spontaneous emission noise, low level feedback does not give an obvious influence on the dynamics, thus, poor consistency of the system enables higher NMSE values. However, with the increase of DC pump, the coherence of laser output is improved. Then, for NMSE value with order of 10^{-2}, the required

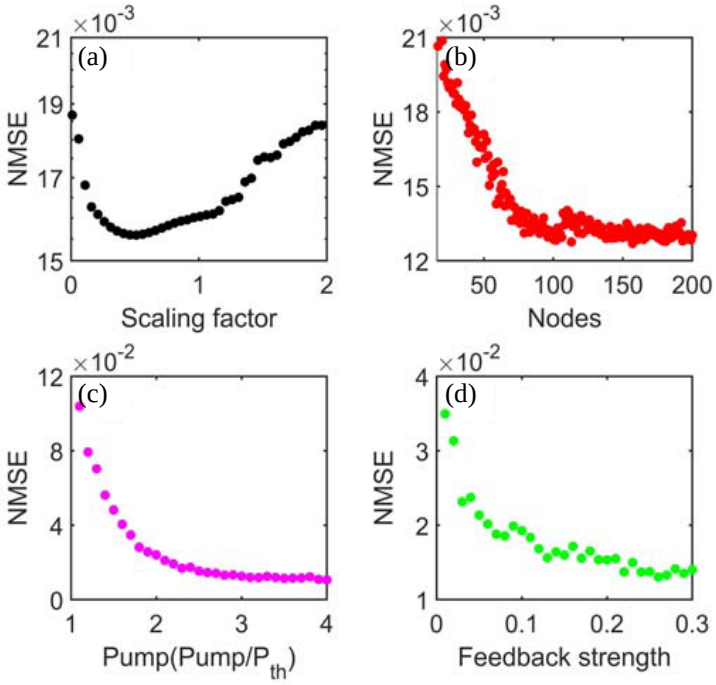

Figure 6. Effects of different parameters on the prediction of Mackey-Glass chaotic sequences: (a) scaling coefficient, (b) number of virtual nodes, (c) injection pump strength and (d) feedback strength.

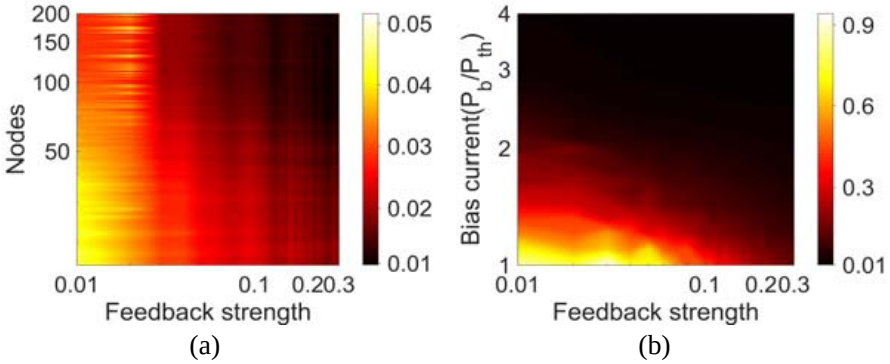

Figure 7. NMSE for the Mackey-Glass chaotic sequences prediction task (a) as a function of feedback strength and virtue node number, also (b) as a function of feedback strength and DC pump using the high-β-laser-based TDRC system.

feedback strength is gradually decreased. When $P_{DC} > 2P_{th}$, a homogeneous NMSE distribution is achievable over a large range of feedback level, which is similar to the task of pattern recognition.

4. MEMORY CAPACITY

We also analyze the memory capacity (MC) property of the system, which is a key indicator for evaluation of TDRC's performance [45, 46]. MC represents the property of the system to retain previously injected information, which is important when the prediction task requires past information, and quantifies the amount of information of past input signals that can be reproduced by the TDRC [47]. For prediction tasks, it is especially important to have information from the past to accurately infer future values, but memory needs to disappear after a period of time so that responses are only influenced

by the latest history, thus it is necessary to discuss MC. MC is usually defined with a correlation function $m(i)$ as follows [48]

$$m(i) = \frac{Cov^2(y_i(n-i), O_i(n))}{\sigma^2(y_i(n))\sigma^2(O_i(n))} \tag{2}$$

where $y_i(n)$ is the injection signal, a pseudo-random sequence between the distributions (0, 1), $O_i(n)$ the sequence of the RC response, Cov the covariance, and $\sigma^2(\,)$ the variance. MC is the sum of $m(i)$:

$$\mathrm{MC} = \sum_{i=1}^{\infty} m(i) \tag{3}$$

Figure 8 shows the calculated correlation functions and MC for the tasks of pattern recognition and Mackey-Glass chaotic sequences prediction. Fig. 8(a) is the correlation function curve $m(i)$ with different prediction steps for pattern recognition. It is clear to see that $m(i)$ keeps high value larger than 0.94, then it tends to be stable with the increase of the prediction step, although there are fluctuations. Fig. 8(b) is the variation of MC with the number of virtual nodes for the task of pattern recognition. Obviously, MC linearly increases with the number of virtual nodes. However, it starts to saturate when $N > 100$. Thus, too many virtual nodes will result in a saturation on the MC, then degrade the prediction performance. Fig. 8(c) and Fig. 8(d) are the corresponding correlation function and MC for the task of Mackey-Glass chaotic sequences prediction. Similar to the pattern recognition task, $m(i)$ tend to be stable after a longer prediction step. The difference is that the values of $m(i)$ are higher than that for the case of pattern recognition, but the MC shows a shorter range of virtual nodes before getting saturation.

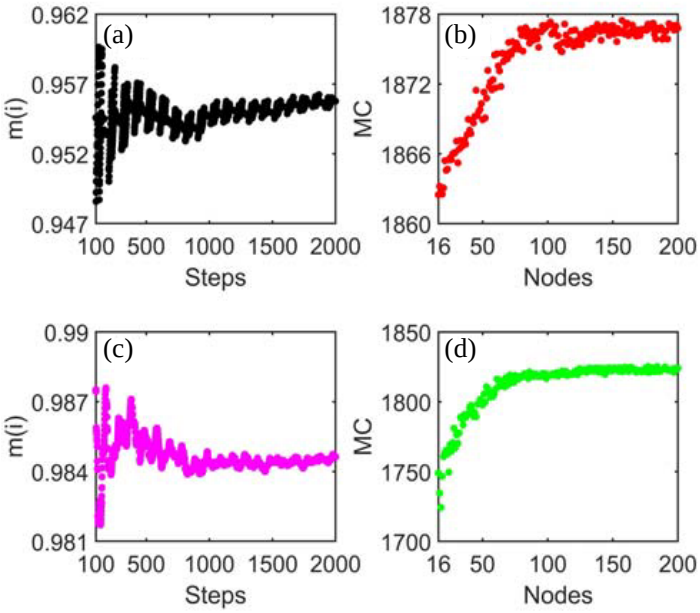

Figure 8. Effects of different parameters on the accuracy of (a), (b) pattern recognition and (c), (d) prediction of Mackey-Glass chaotic sequences: for pattern recognition, (a) prediction steps, (b) number of virtual nodes; for the prediction of Mackey-Glass chaotic sequences, (c) prediction steps and (d) number of virtual nodes.

5. INFLUENCE OF SPONTANEOUS EMISSION NOISE

Finally, in order to fully understand the influence of the spontaneous noise on the performance of TDRC system for different tasks, we conduct evaluations at $P_{DC} = 1.5P_{th}$, $2.0P_{th}$, and $2.5P_{th}$, respectively, and calculate the corresponding MC function curves with virtual node number. Typically, when we

increase the DC pump, the laser emission becomes more coherent, and the number of spontaneous photons decreases. By adjusting the DC pump, we can change the amount of spontaneous noise within the system and study how it affects the overall performance of the TDRC.

As shown in Fig. 9(a), for the task of prediction of Mackey-Glass chaotic sequences, the variation of DC pump has no obvious influence on the MC value in the region of $N \leq 50$. Therefore, the addition of noise does not affect the performance of TDRC when making predictions. However, there are noticeable deviations between the function curves when $N > 50$, and higher MC values are observed when using high DC pump. The results indicate that using fewer noises could potentially lead to a better performance. For the case of pattern recognition, as shown in Fig. 9(b), the presence of spontaneous noise can have a significant impact on the MC value. It is clear to see that even before the saturation of MC, the negative effects of spontaneous noise on the performance of the TDRC are noticeable. This is particularly relevant since pattern recognition tasks tend to be more sensitive to noise, and the presence of spontaneous noise can make it more challenging to achieve accurate results. Therefore, it is essential to take spontaneous noise into account when designing and implementing TDRC systems for pattern recognition tasks, to ensure optimal accuracy and performance.

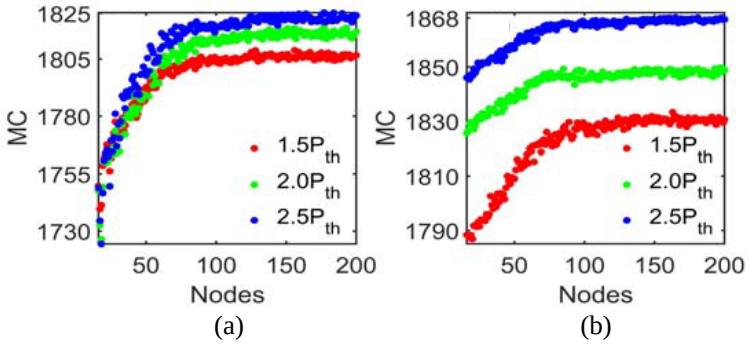

Figure 9. Calculated MC function curves for (a) prediction of Mackey-Glass chaotic sequences and (b) pattern recognition tasks at $P_{DC} = 1.5P_{th}$, $2.0P_{th}$, and $2.5P_{th}$, respectively.

6. CONCLUSIONS

In summary, we have proposed a TDRC system based on the dynamics of threshold region of a high-β semiconductor laser with delayed optical feedback and carried out numerical studies on the performance for the tasks of pattern recognition and Mackey-Glass chaotic sequence prediction. Due to the unique feature of spiking dynamics in transition region, we find that semiconductor high-β lasers display promising potentials for the TDRC system. Within the study, we pay special attention to the influence of the scaling factor, DC pump of the laser, virtual node number, and feedback strength on the prediction performance, and show it in the form of a mapping graph. The results show that the increase of those parameters within a certain range can significantly improve the prediction performance of the TDRC system. Therefore, properly adjusting those parameters is particularly important for TDRC to improve the prediction performance, thus, reducing the cost and the calculation time.

We have analyzed the MC properties for these two tasks, and the results indicate that with the increase of the number of virtual nodes, MCs are significantly improved. However, they tend to be stable after a certain range. This phenomenon explains that continual increasing the number of virtual nodes cannot further improve the prediction performance of TDRC. Besides, we have also investigated how laser noise affects the performance of the TDRC system in terms of pattern recognition and Mackey-Glass chaotic sequence prediction. The results showed that the spontaneous noise had a significant negative impact on the overall performance of the TDRC system. Moreover, we found that the task of pattern recognition was more adversely affected by the spontaneous noise than chaotic sequence prediction. This indicates that the noise reduction should be considered to improve the performance of the TDRC system for applications that require high accuracy in pattern recognition. Our proposed TDRC system may hold promising potentials for the future on-chip reservoir computing.

ACKNOWLEDGMENT

The authors are grateful to the anonymous referees for constructive criticism and useful suggestions, which have improved the quality of the manuscript. They also thank to Prof. Gian Luca and Dr. Gian Piero Puccioni for fruitful discussions. This work is partially supported by several sources: National Key Research and Development Program of China (2021YFB2801900, 2021YFB2801901, 2021YFB2801902, 2021YFB2801904), National Natural Science Foundation of China (Grant No. 61804036), Zhejiang Province Commonweal Project (Grant No. LGJ20A040001), National Key R & D Program Grant (Grant No. 2018YFE0120000), Zhejiang Provincial Key Research & Development Project Grant (Grant No. 2019C04003).

REFERENCES

1. Qian, C., B. Zheng, Y. Shen, L. Jing, E. Li, L. Shen, and H. Chen, "Deep-learning-enabled self-adaptive microwave cloak without human intervention," *Nat. Photonics*, Vol. 14, 383–390, 2020.
2. Jia, Y., C. Qian, Z. Fan, T. Cai, E. Li, and H. Chen, "A knowledge-inherited learning for intelligent metasurface design and assembly," *Light: Science & Applications*, Vol. 12, 82, 2023.
3. Zhang, J., C. Qian, J. Chen, B. Wu, and H. Chen, "Uncertainty qualification for metasurface design with amendatory Bayesian network," *Laser & Photonics Reviews*, 2200807, 2023.
4. Maass, W., T. Natschläger, and H. Markram, "Real-time computing without stable states: A new framework for neural computation based on perturbations," *Neural Comput.*, Vol. 14, No. 11, 2531–2560, 2002.
5. Jaeger, H. and H. Haas, "Harnessing nonlinearity: Predicting chaotic systems and saving energy in wireless communication," *Science*, Vol. 304, No. 5667, 78–80, 2004.
6. Der Sande, G. V., D. Brunner, and M. C. Soriano, "Advances in photonic reservoir computing," *Nanophotonics*, Vol. 6, No. 3, 561–576, 2017.
7. Guo, X. X., S. Y. Xiang, Y. H. Zhang, L. Lin, A. J. Wen, and Y. Hao, "Four-channels reservoir computing based on polarization dynamics in mutually coupled VCSELs system," *Opt. Express*, Vol. 27, No. 16, 23293–23306, 2019.
8. Vandoorne, K., J. Dambre, D. Verstraeten, B. Schrauwen, and P. Bienstman, "Parallel reservoir computing using optical amplifiers," *IEEE Transactions on Neural Networks*, Vol. 22, No. 9, 1469–1481, 2011.
9. Takano, K., C. Sugano, M. Inubushi, K. Yoshimura, S. Sunada, K. Kanno, and A. Uchida, "Compact reservoir computing with a photonic integrated circuit," *Opt. Express*, Vol. 26, No. 22, 29424–29439, 2018.
10. Vatin, J., D. Rontani, and M. Sciamanna, "Enhanced performance of a reservoir computer using polarization dynamics in VCSELs," *Opt. Lett.*, Vol. 43, No. 18, 4497–4500, 2018.
11. Appeltant, L., M. C. Soriano, G. van der Sande, J. Danckaert, S. Massar, J. Dambre, B. Schrauwen, C. R. Mirasso, and I. Fischer, "Information processing using a single dynamical node as complex system," *Nature Commun.*, Vol. 2, 468, 2011.
12. Brunner, D., M. C. Soriano, C. R. Mirasso, and I. Fischer, "Parallel photonic information processing at gigabyte per second data rates using transient states," *Nature Commun.*, Vol. 4, 1364, 2013.
13. Ortín, S. and L. Pesquera, "Reservoir computing with an ensemble of time-delay reservoirs," *Cogn. Comput.*, Vol. 9, No. 3, 327–336, 2017.
14. Goldmann, M., F. Köster, K. Lüdge, and S. Yanchuk, "Deep time-delay reservoir computing: Dynamics and memory capacity," *Chaos*, Vol. 30, 093124, 2020.
15. Stelzer, F., A. Röhm, K. Lüdge, and S. Yanchuk, "Performance boost of time-delay reservoir computing by non-resonant clock cycle," *Neural Networks*, Vol. 124, 158–169, 2020.
16. Vatin, J., D. Rontani, and M. Sciamanna, "Experimental reservoir computing using VCSEL polarization dynamics," *Opt. Express*, Vol. 27, 18579–18584, 2019.

17. Soriano, M. C., S. Ortín, L. Keuninckx, L. Appeltant, J. Danckaert, L. Pesquera, and G. van der Sande, "Delay-based reservoir computing: Noise effects in a combined analog and digital implementation," *IEEE Trans. Neural Netw. Learn. Syst.*, Vol. 26, No. 2, 388–393, 2015.
18. Larger, L., M. C. Soriano, D. Brunner, L. Appeltant, J. M. Gutierrez, L. Pesquera, C. R. Mirasso, and I. Fischer, "Photonic information processing beyond turing: An optoelectronic implementation of reservoir computing," *Opt. Express*, Vol. 20, No. 3, 3241–3249, 2012.
19. Hülser, T., F. Koster, K. Ludge, and L. Jaurigue, "Deriving task specific performance from the information processing capacity of a reservoir computer," *Nanophotonics*, Vol. 12, 937–947, 2023.
20. Chen, Y., L. Yi, J. Ke, Z. Yang, Y. Yang, L. Huang, Q. Zhuge, and W. Hu, "Reservoir computing system with double optoelectronic feedback loops," *Opt. Express*, Vol. 27, No. 20, 27431–27440, 2019.
21. Li, Z., S. S. Li, X. Zou, W. Pan, and L. Yan, "Processing-speed enhancement in a delay-laser-based reservoir," *Photonics*, Vol. 9, 240, 2022.
22. Chemboa, Y. K., "Machine learning based on reservoir computing with time-delayed optoelectronic and photonic systems," *Chaos*, Vol. 30, 013111, 2020.
23. Ashner, M. N., U. Paudel, M. Luengo-Kovac, J. Pilawa, T. Justin Shaw, and G. C. Valley, "Photonic reservoir computer with all-optical reservoir," *Proc. SPIE, AI and Optical Data Sciences II*, 117030L, 2021.
24. Skontranis, M., G. Sarantoglou, A. Bogris, and C. Mesaritakis, "Time-delayed reservoir computing based on a dual-waveband quantum-dot spin polarized vertical cavity surface-emitting laser," *Optical Materials Express*, Vol. 12, 4047–4060, 2022.
25. Chen, P., R. Liu, K. Aihara, and L. Chen, "Autoreservoir computing for multistep ahead prediction based on the spatiotemporal information transformation," *Nature Commun.*, Vol. 11, 4568, 2020.
26. Xu, Y., M. Zhang, L. Zhang, P. Lu, S. Mihailov, and X. Bao, "Time-delay signature suppression in a chaotic semiconductor laser by fiber random grating induced random distributed feedback," *Opt. Lett.*, Vol. 42, 4107–4110, 2017.
27. Zhang, L., B. Pan, G. Chen, L. Guo, D. Lu, L. Zhao, and W. Wang, "640-Gbit/s fast physical random number generation using a broadband chaotic semiconductor laser," *Sci. Rep.*, Vol. 7, 45900, 2017.
28. Estébanez, I., J. Schwind, I. Fischer, and A. Argyris, "Accelerating photonic computing by bandwidth enhancement of a time-delay reservoir," *Nanophotonics*, Vol. 9, No. 13, 4163–4171, 2020.
29. Wang, T., X. Wang, Z. Deng, J. Sun, G. P. Puccioni, G. Wang, and G. L. Lippi, "Dynamics of a micro-VCSEL operated in the threshold region under low-level optical feedback," *IEEE J. Sel. Top. Quantum Electron.*, Vol. 25, 1700308, 2019.
30. Wang, T. and G. L. Lippi, "Polarization-resolved cartography of light emission of a vertical-cavity surface-emitting laser with high space and frequency resolution," *Appl. Phys. Lett.*, Vol. 107, 181103, 2015.
31. Torre, M. S., C. Masoller, P. Mandel, and K. A. Shore, "Enhanced sensitivity to current modulation near dynamic instability in semiconductor lasers with optical feedback and optical injection," *J. Opt. Soc. Am. B*, Vol. 21, 302–306, 2004.
32. Nazhan, S., Z. Ghassemlooy, K. Busawon, and A. Gholami, "Investigation of polarization switching of VCSEL subject to intensity modulated and optical feedback," *Optics & Laser Technology*, Vol. 75, 240–245, 2015.
33. Deng, H., G. L. Lippi, J. Mork, J. Wiersig, and S. Reitzenstein, "Physics and applications of high-β micro- and nanolasers," *Adv. Optical Mater.*, Vol. 9, 2100415, 2021.
34. Javanshir, A., T. T. Nguyen, M. A. Parvez Mahmud, and A. Z. Kouzani, "Advancements in algorithms and neuromorphic hardware for spiking neural networks," *Neural Comput.*, Vol. 34, No. 6, 1289–1328, 2022.
35. Wang, T., G. P. Puccioni, and G. L. Lippi, "Dynamical buildup of lasing in mesoscale devices," *Scientific Reports*, Vol. 5, 15858, 2015.

36. Wang, T., C. Jiang, J. Zou, J. Yang, K. Xu, C. Jin, G. Wang, G. P. Puccioni, and G. L. Lippi, "Nanolasers with feedback as low-coherence illumination sources for speckle-free imaging: A numerical analysis of the superthermal emission regime," *Nanomaterials*, Vol. 11, 3325, 2021.
37. Brunner, D., L. Larger, and M. C. Soriano, "Nonlinear photonic dynamical systems for unconventional computing," *Nonlinear Theory and Its Applications, IEICE*, Vol. 13, 26–35, 2022.
38. Puccioni, G. P. and G. L. Lippi, "Stochastic Simulator for modeling the transition to lasing," *Opt. Express*, Vol. 23, No. 3, 2369–2374, 2015.
39. Lippi, G. L., T. Wang, and G. P. Puccioni, "'Phase transitions' in small systems: Why standard threshold definitions fail for nanolasers," *Chaos, Solitons and Fractals*, Vol. 157, 111850, 2022.
40. Rice, P. R. and H. J. Carmichael, "Photon statistics of a cavity-QED laser: A comment on the laser-phase-transition analogy," *Phys. Rev. A*, Vol. 50, 4318, 1994.
41. Guo, X. X., S. Y. Xiang, Y. H. Zhang, L. Lin, A. J. Wen, and Y. Hao, "High-speed neuromorphic reservoir computing based on a semiconductor nanolaser with optical feedback under electrical modulation," *IEEE J. Sel. Top. Quantum Electron.*, Vol. 26, 1500707, 2020.
42. Brunner, D., M. C. Soriano, C. R. Mirasso, and I. Fischer, "Parallel photonic information processing at gigabyte per second data rates using transient states," *Nature Commun.*, Vol. 4, 1364, 2013.
43. Yue, D., Z. Wu, Y. Hou, B. Cui, Y. Jin, M. Dai, and G. Xia, "Performance optimization research of reservoir computing system based on an optical feedback semiconductor laser under electrical information injection," *Opt. Exp.*, Vol. 27, No. 14, 19931–19939, 2019.
44. Yue, D., Y. Hou, Z. Wu, C. Hu, Z. Xiao, and G. Xia, "Experimental investigation of an optical reservoir computing system based on two parallel time-delay reservoirs," *IEEE Photonics Journal*, Vol. 13, No. 3, 8500111, 2021.
45. Köster, F., S. Yanchuk, and K. Lüdge, "Insight into delay based reservoir computing via eigenvalue analysis," *J. Phys. Photonics*, Vol. 3, 024011, 2021.
46. Hülser, T., F. Köster, L. Jaurigue, and K. Lüdge, "Role of delay-times in delay-based photonic reservoir computing," *Opt. Mater. Express*, Vol. 12, 1214–1231, 2022.
47. Sugano, C., K. Kanno, and A. Uchida, "Reservoir computing using multiple lasers with feedback on a photonic integrated circuit," *IEEE J. Sel. Topics Quantum Electron.*, Vol. 26, No. 1, 1–9, 2020.
48. Taylor, J., *Introduction to Error Analysis. The Study of Uncertainties in Physical Measurements*, 2nd Edition, 349 (cit. on p. 84), University Science Books, Sausalito, California, 1997.